EPJ Web of Conferences **126**, 04011 (2016) DOI: 10.1051/epjconf/201612604011
ICNFP 2015

Single top-quark production cross-section and properties using the ATLAS detector at the LHC

Andrew M. Chegwidden[1,a], On behalf of the ATLAS Collaboration

[1] *Department of Physics and Astronomy, Michigan State University*

Abstract. ATLAS measurements of single top-quark processes are summarised. Measurements using data recorded at the LHC proton-proton collider at centre-of-mass energies of $\sqrt{s}$=7 TeV and 8 TeV are presented. The measurements are performed using the semi-leptonic decay mode of the top quark. Production cross-sections for the t-channel and Wt modes of single top-quark production and the extraction of the CKM matrix element $|V_{tb}|$ are shown. All measurements are compared to theoretical calculations. In addition, the s-channel production mode is explored along with limits on exotic production modes.

1 Introduction

Studying single top-quark processes allows for both a further understanding of the Standard Model (SM) as well as a probe for beyond the Standard Model (BSM) theories. Single top-quark processes also allow for unique tests of the SM. The ratio of the parton distribution functions (PDF) for the up and down quarks and the CKM matrix element $|V_{tb}|$ are easily extracted from measurements of single top-quark production cross-sections. Many BSM searches utilise single top-quark final states as their signature or as a background. These proceedings present measurements of single top-quark processes in proton-proton (pp) collisions at centre-of-mass energies of $\sqrt{s}$=7 TeV and 8 TeV using data recorded by the ATLAS detector [1] at the LHC [2].

2 Measurements

The production of single top quarks at the LHC occurs through three relevant subprocesses: t-channel production where a space-like W boson is exchanged, associated production of a top-quark and an on-shell W boson (Wt-channel), and s-channel production which is mediated by an off-shell W boson.

[a] e-mail: andrew.chegwidden@cern.ch

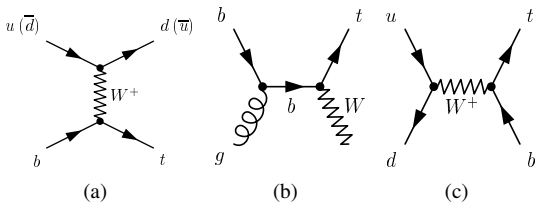

Figure 1. Feynman diagrams of single top-quark production processes: (a) t-channel production, (b) associated Wt production, and (c) s-channel production.

The Feynman diagrams for these processes are shown in Figure 1.

2.1 Measurement of the t-channel cross-section

The t-channel production mode is the dominant single top production mode at the LHC. The t-channel cross-section is predicted at next-to-leading order with next-to-next-to-leading logarithm gluon resummation. They are calculated to be $\sigma_t = 64.6.8^{+2.6}_{-1.7}$ pb and $\sigma_t = 87.8^{+3.4}_{-1.9}$ pb for $\sqrt{s}$=7 TeV and $\sqrt{s}$=8 TeV, respectively [3]. The analysis uses the semi-leptonic decay of the W boson such that the final state consists of two high-p_{T} jets (one forward light-quark from the initial hard scatter and one central b-tagged jet from the W decay), one isolated high p_{T} lepton, and large $E_{\mathrm{T}}^{\mathrm{miss}}$. This selection is applied to reconstructed events and is also used to define a fiducial region based on particle-level objects. Signal discrimination from background events is enhanced through the use of a neural-network (NN) based on 14 final state variables. The two most discriminating variables are the pseudorapidity[1] of the untagged jet $|\eta(j)|$ and the reconstructed mass of the top-quark $m(\ell\nu b)$.

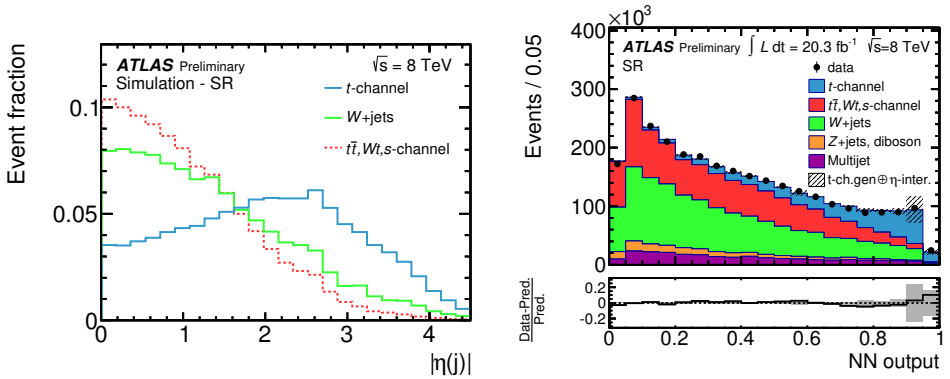

Figure 2. Distributions of the (a) most discriminating variable, the η of the untagged jet and of (b) the NN output-distribution for the combined electron and muon channel are shown. The shaded band includes the t-channel generator uncertainty and the jet energy scale η-intercalibration uncertainty. The Signal Region (SR) corresponds to events with exactly one lepton, missing transverse momentum, and exactly one b-tagged jet [4].

[1] ATLAS uses a right-handed coordinate system with its origin at the nominal interaction point (IP) in the centre of the detector and the z-axis along the beam pipe. The x-axis points from the IP to the centre of the LHC ring, and the y-axis points upward. Cylindrical coordinates (r, ϕ) are used in the transverse plane, ϕ being the azimuthal angle around the beam pipe. The pseudorapidity is defined in terms of the polar angle θ as $\eta = -\ln\tan(\theta/2)$.

The $|\eta(j)|$ distribution and the output of the NN can bee seen in Figures 2(a) and 2(b), respectively [4]. The estimated number of t-channel single top-quark events is obtained from a binned maximum-likelihood fit of the NN output and is used to calculate a fiducial cross-section. The fiducial cross-section is calculated using the inclusive cross-section for each MC generator and the corresponding selection efficiency of the particle-level selection. A fiducial cross-section of $\sigma_{\text{fid}} = 3.37 \pm 0.05(\text{stat}) \pm 0.48(\text{syst})$ pb is obtained [4].

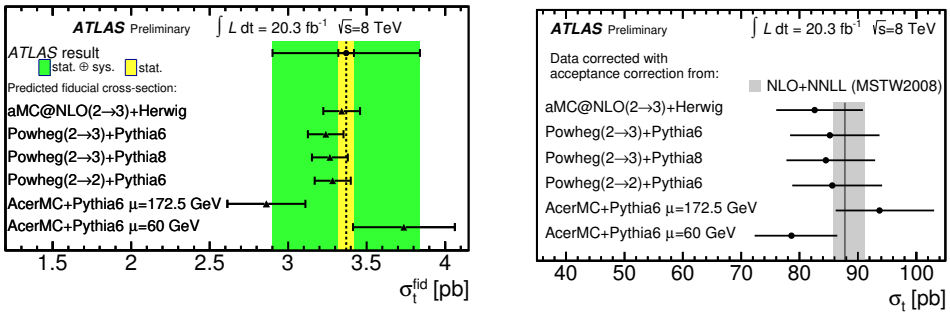

(a) (b)

Figure 3. (a) The t-channel fiducial cross-section predictions for different NLO MC generators together with the measured value and (b) the total t-channel cross-section measurements obtained from the fiducial cross-section using the acceptance of different MC generators [4].

Figure 3(a) shows the extrapolation of the fiducial cross-section to the full phase space using the acceptance from various MC generator models while Figure 3(b) shows the extrapolated inclusive cross-section [4]. Using the acceptance of the fiducial volume from the aMC@NLO + Herwig event generator [5], an inclusive t-channel cross-section of $\sigma_t = 82.6 \pm 1.2(\text{stat}) \pm 11.4(\text{syst})$ pb is obtained [4].

2.2 Measurement of the Wt-channel cross-section

The associated production of a top quark and a W boson is the second-largest production mode of single top events at the LHC. The Wt-channel cross-section is predicted at next-to-leading order with next-to-next-to-leading logarithm gluon resummation. They are calculated to be $\sigma_{Wt} = 15.74^{+1.17}_{-1.21}$ pb and $\sigma_{Wt} = 22.37 \pm 1.52$ pb for $\sqrt{s}$=7 TeV and $\sqrt{s}$=8 TeV, respectively [6]. The analysis uses events with a final state consisting of one electron, one oppositely charged muon, $E_{\text{T}}^{\text{miss}}$, and at least one b-tagged central jet. Signal discrimination from background events is enhanced through the use of a Boosted Decision Tree (BDT) classifier.

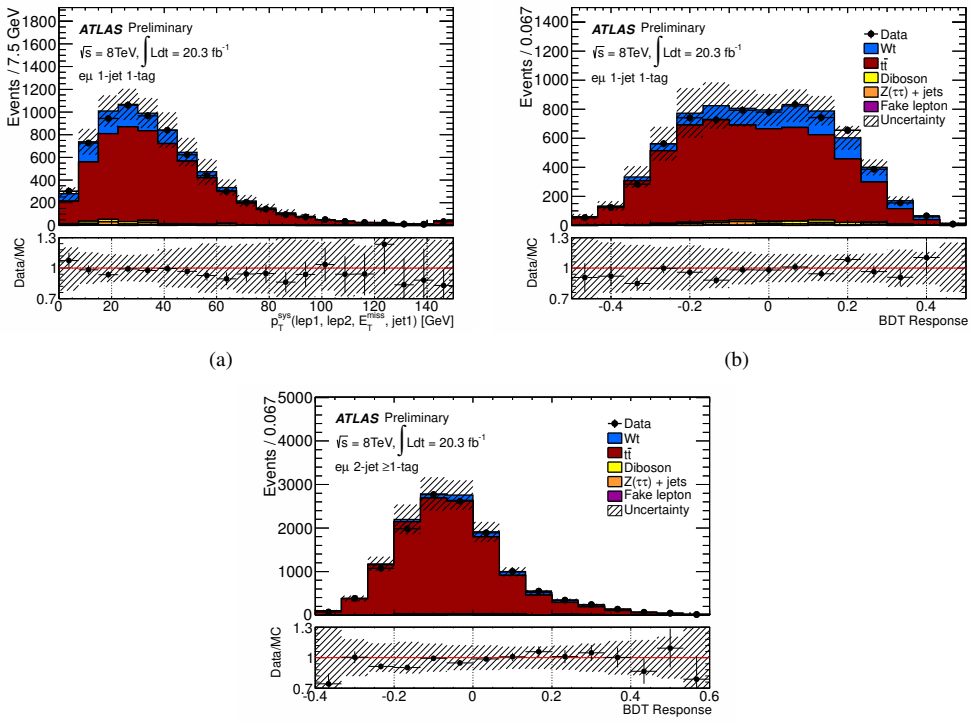

Figure 4. (a) Distribution of the the p_{T} of the vectorial sum of the leptons, $E_{\mathrm{T}}^{\mathrm{miss}}$, and the leading jet. BDT classifier distributions for (b) 1-jet and (c) 2-jet events. The uncertainty band is the quadratic sum of all systematic uncertainties [7].

Of the 19 variables used in the analysis, the one with the highest discriminating power is shown in Figure 4(a). Classifiers are trained for both 1-jet and 2-jet events. The outputs for the 1-jet and 2-jet classifiers are shown in Figures 4(b) and 4(c), respectively. A maximum-likelihood fit to the BDT classifier distributions is performed to extract the signal cross-section. The result of the fit is a Wt-channel cross-section measurement of $\sigma_{Wt} = 27.2 \pm 2.8(\mathrm{stat}) \pm 5.4(\mathrm{syst})$ pb [7].

2.3 CKM matrix element $|Vtb|$

Single top-quark production in the t- and Wt-channels proceeds via the W-t-b vertex. As such, the cross-section for the production modes is proportional to $|V_{tb}|^2$. The SM predicts $|V_{tb}|$ to be close to 1.0 and its value is sensitive to new physics such as additional quark generations. Measurements of $|V_{tb}|$ are independent of the assumption of the number of quark generations as well as the unitarity of the CKM matrix. The only assumptions made are that $|V_{tb}| \gg |V_{td}|$, $|V_{ts}|$, meaning $\mathcal{B}(t \to bW) = 1$, and that the W-t-b vertex is a SM-like weak coupling. The observed value of $|V_{tb}|^2$ is calculated by dividing the measured cross-section by the theoretical prediction,

$$|V_{tb} \cdot f|^2 = \frac{\sigma_{\mathrm{exp}}}{\sigma_{\mathrm{theory}}} \tag{1}$$

and with a fixed top-quark mass of 172.5 GeV. In Equation (1), f is a coupling which is allowed to be bigger than the SM value of 1. The values of $|V_{tb} \cdot f|$ extracted from the t- and Wt-channel cross-sections are $|V_{tb}| = 0.97^{+0.09}_{-0.10}$ [4] and $|V_{tb}| = 1.10 \pm 0.12$ [7], respectively. Lower limits on the value of $|V_{tb}|$ at the 95% confidence level using the t- and Wt-channel production cross-sections are $|V_{tb}| > 0.78$ [4] and $|V_{tb}| > 0.72$ [7], respectively.

3 SM and BSM searches

Many BSM searches have been conducted at the LHC involving events having final states similar to that of single top-quark processes. While the s-channel production mode has been observed at the Tevatron, it has proven difficult to observe at the LHC. Searches involving additional heavy gauge bosons and dark matter candidates have also been conducted.

3.1 Search for SM s-channel production

Single top-quark production in the s-channel was first observed at the Tevatron in proton-antiproton ($p\bar{p}$) collisions by the CDF and D0 collaborations [8]. Measuring the s-channel production mode at the LHC is difficult as the signal-to-background ratio is much smaller in pp collisions than in $p\bar{p}$ collisions due to the quark-antiquark initial state. The s-channel cross-section is predicted at next-to-leading order with next-to-next-to-leading logarithm gluon resummation. They are calculated to be $\sigma_s = 4.63^{+0.20}_{-0.18}$ pb and $\sigma_s = 5.61 \pm 0.22$ pb for $\sqrt{s}$=7 TeV and $\sqrt{s}$=8 TeV, respectively [9]. The analysis selects events with a single lepton, exactly two b-tagged jets, and large $E_{\mathrm{T}}^{\mathrm{miss}}$. To discriminate between signal and background events, a BDT event classifier is utilised. Nineteen final state variables are used as input to the BDT such that the expected signal significance is maximised. The variable with the highest discriminating power is the difference in azimuthal angle between the leading b-tagged jet and the top-quark candidate reconstructed with the sub-leading b-tagged jet.

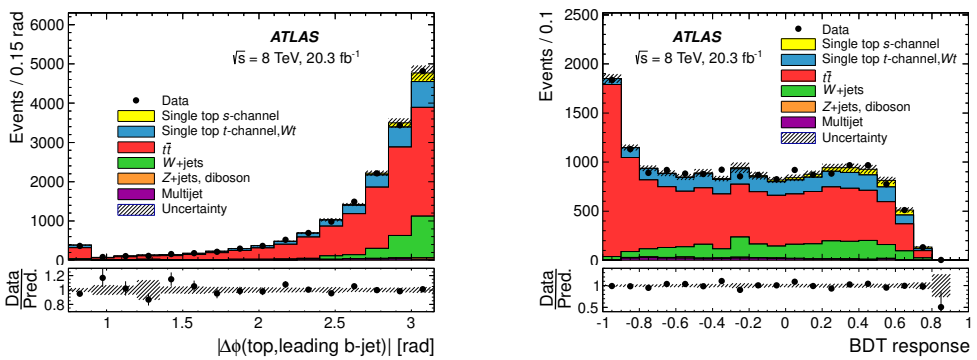

(a) (b)

Figure 5. Distributions of (a) the most discriminating variable used in BDT classifier, the $|\Delta\phi|$ between the leading b-tagged jet and the top-quark candidate reconstructed with the sub-leading b-tagged jet and (b) observed and predicted values of the BDT response. The uncertainty band represent the normalisation uncertainty of all processes after the fit and added in quadrature with Monte Carlo statistical uncertainty [10].

Distributions of the most discriminating variable and of the BDT output are shown in Figures 5(a) and 5(b), respectively. The signal is extracted in a binned maximum-likelihood fit of the BDT output

distribution. The fit gives a cross-section of $\sigma_s = 5.0 \pm 4.3$ pb, which is consistent with the SM. The observed upper limit on the s-channel cross-section is 14.6 pb at the 95% CL [10].

3.2 Search for additional heavy gauge bosons, W'

The single top-quark final state can be used to search for additional charged heavy gauge bosons. The analysis performs a search in the $W' \to t\bar{b} \to \ell\nu b\bar{b}$ decay mode. This process is similar to the SM s-channel production mode except it is mediated by the W', a heavier version of the W boson. The analysis utilises a BDT classifier in order to discriminate signal from background. Four BDTs are trained for two-jet and three-jet multiplicity events and W' boson signals with left-handed and right-handed couplings to the top quark. Ten (eleven) variables are used as inputs in the BDT in 2-jet (3-jet) searches. Of these variables, $m_{t\bar{b}}$ and $p_{\mathrm{T}}(t)$ have the highest discriminating power.

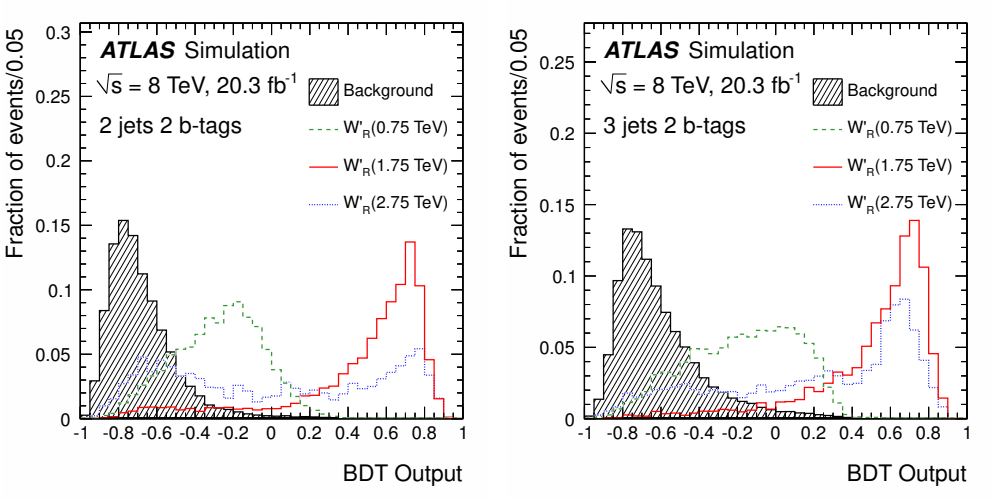

(a) (b)

Figure 6. Distributions of the BDT output for three different mass hypotheses of the W'_R boson in (a) the 2-jet and (b) the 3-jet multiplicity signal regions. Electron and muon channels are combined and all distributions are normalised to unity [11].

The BDT outputs for 2-jet and 3-jet multiplicity events are shown in Figures 6(a) and 6(b) respectively. As no excess in data is observed, exclusion limits are set. For a left-handed (right-handed) W' boson, masses below 1.70 (1.92) TeV are excluded at the 95% CL [11].

3.3 Monotop

Many BSM theories predict the production of events with large missing transverse momentum in association with a single reconstructed object. Such searches are colloquially known as Mono-X searches and have taken place at the LHC where the single object is taken to be a photon, a heavy quark, or a W or Z boson. The monotop analysis follows the spirit of these searches where the final state consists of a singly-produced top quark in association with a significant amount of missing transverse momentum. This missing transverse momentum could correspond to one or several undetected neutral particles.

These particles can either be stable or weakly interacting and can be interpreted as dark matter candidates. The analysis considers two main production modes. The first is the resonant production of a +2/3 charged spin-0 boson, S, decaying into a right-handed top-quark and a neutral colour-singlet spin-1/2 fermion, f_{met}. The second is the non-resonant production of a neutral, color singlet, spin-1 boson, v_{met}, in association with a right-handed top-quark.

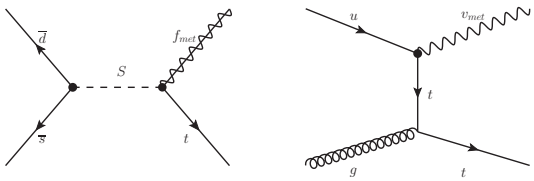

(a) (b)

Figure 7. Feynman diagrams of leading-order processes leading to monotop events through (a) the production of a colored scalar resonance S decaying into a top-quark and a spin-1/2 fermion f_{met} in the resonant model and (b) the t-channel non-resonant production of a top quark in association with a spin-1 boson v_{met} in the non-resonant model [12].

The Feynman diagrams for these two production modes are shown in Figure 7. The analysis utilises a cut-based approach for the discrimination of the signal from the background. The monotop signal is prominent in regions of phase space characterised by high transverse mass calculated with the lepton and missing transverse momentum, $m_{\text{T}}(\ell, E_{\text{T}}^{\text{miss}})$, as well as small values of $|\Delta\phi(\ell, b)|$.

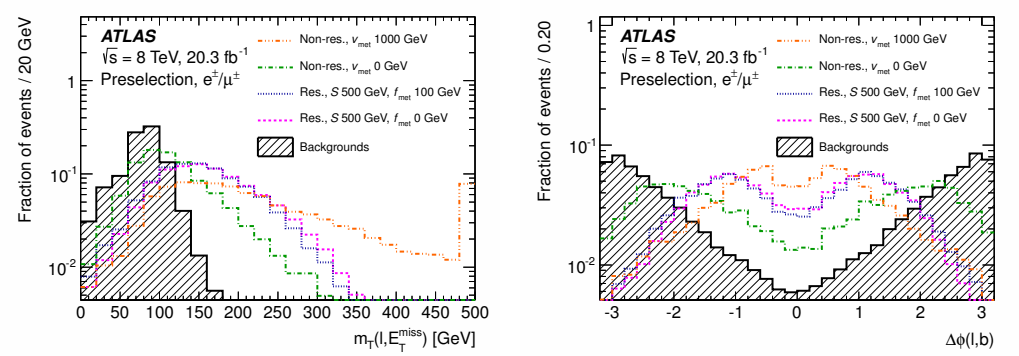

(a) (b)

Figure 8. Distributions normalised to unity of (a) $m_{\text{T}}(\ell, E_{\text{T}}^{\text{miss}})$ and of (b) $|\Delta\phi(\ell, b)|$. The expected distributions for the resonant model with $m(S) = 500$ GeV are shown for the $m(f_{\text{met}}) = 0$ GeV and $m(f_{\text{met}}) = 100$ GeV hypotheses, as well as for the non-resonant model for the $m(v_{\text{met}}) = 0$ GeV and $m(v_{\text{met}}) = 1000$ GeV hypotheses. All distributions are compared to the expected distribution for the backgrounds [12].

Figure 8 shows the distribution of the two variables used in the analysis to discriminate signal from background. As no excess is observed in data, 95% CL upper limits on the signal production cross-sections are set.

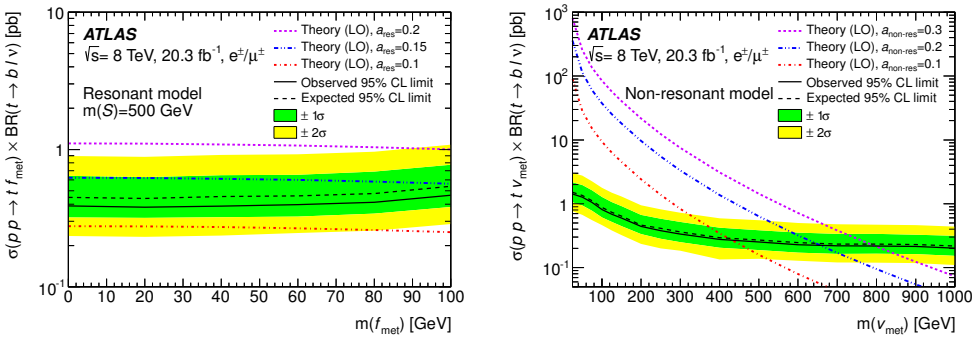

(a) (b)

Figure 9. Observed and expected limits on the cross-section times branching ratio for the (a) resonant model with $m(S) = 500$ GeV and (b) non-resonant model, as a function of $m(f_{\text{met}})$ and $m(v_{\text{met}})$, respectively [12].

Figure 9 shows the limit at the 95% CL on the production cross-section times branching ratio as a function of the invisible state, for each of the two signal models. In the case of resonant production, cross-sections are excluded across the entire mass range. In the non-resonant production mode, cross-sections up to $m(v_{\text{met}}) = 657$ GeV are excluded [12].

4 Summary

Single top-quark measurements and properties were presented along with current limits on exotics production modes and an upper limit on the SM s-channel production cross-section. Single top-quark events continue to serve as a test of the SM as well as a probe for BSM theories. Many new results should be forthcoming as data are collected from $\sqrt{s}$=13 TeV collisions.

Acknowledgments

The author wishes to thank the organisers for the invitation and gratefully acknowledges the support of the National Science Foundation (grant PHY-1068318).

References

[1] ATLAS Collaboration, JINST **3** (2008) S08003.
[2] L. Evans and P. Bryant (editors), JINST **3** (2008) S08001.
[3] N. Kidonakis,Phys.Rev.D **83** (2011) 091503.
[4] ATLAS Collaboration, ATLAS-CONF-2014-007, http://cds.cern.ch/record/1668960 .
[5] G. Corcella et al., JHEP 0101 (2001) 010.
[6] N. Kidonakis,Phys.Rev.D **82** (2010) 054018.
[7] ATLAS Collaboration, ATLAS-CONF-2013-100, http://cds.cern.ch/record/1600799 .
[8] CDF and D0 Collaborations, T. Aaltonen et al, Phys.Rev.Lett. **112** (2014) 231803.
[9] N. Kidonakis, Phys.Rev.D **81** (2010) 054028.
[10] ATLAS Collaboration, Phys.Lett.B **740** (2014) 118.
[11] ATLAS Collaboration, Phys.Lett.B **743** (2015) 233-255.
[12] ATLAS Collaboration, EPJC **75** (2015) 79.